NOTATION

v and w, radial and axial velocity components of the medium, respectively; r and z, radial and axial coordinates, respectively; k, suction intensity at the disk surface; ρ, density; η and ν, dynamic and kinematic viscosity coefficients of the medium, respectively; c_p, specific heat; κ, thermal conductivity; σ, conductivity; B, magnetic induction; T, temperature; ω, angular velocity of the disk; R, disk radius.

LITERATURE CITED

1. V. D. Borisevich and E. P. Potanin, Inzh.-Fiz. Zh., 49, No. 6, 1022-1026 (1985).
2. V. D. Borisevich and E. P. Potanin, Izv. Akad. Nauk SSSR, Mekh. Zhidk. Gaza, No. 4, 177-181 (1985).
3. E. M. Sparrow and R. D. Cess, Trans. ASME, J. Appl. Mech., 84, 181-187 (1962).
4. V. D. Borisevich and E. P. Potanin, Magn. Gidrodin., No. 1, 135-137 (1987).
5. P. Bar-Yoseph and S. Olek, Comput. Fluids, 12, No. 3, 177-197 (1984).
6. L. G. Loitsyanskii, Laminar Boundary Layer [in Russian], Moscow (1962).

DYNAMICS OF MACROMOLECULES IN CONVERGENT-CHANNEL FLOWS

Z. P. Shul'man, É. A. Zal'tsgendler, and B. M. Khusid

UDC 532.135

The deformation of flexible and rigid macromolecules is analyzed under conditions of convergent-channel flows.

Certain pieces of equipment employed in chemical technology as well as in biotechnology make use of a dispersion medium to compress the stream of a macromolecular solution. For this case it is necessary to evaluate the effect of the shape of the convergent nozzle, the rate of flow, and the characteristics of the macromolecules on the deformation which takes place during the flow in the convergent channel and after passage through the channel (Fig. 1). The simplest of macromolecules have been used for these calculations, i.e., in the shape of flexible dumbbells and rigid axisymmetric ellipsoids. The deformation of the macromolecular flow near the axis of the convergent channel is close to elongational (the radius of the stream of the solution is considerably smaller than the radius of the convergent channel).

Flexible Macromolecules. The behavior of flexible macromolecules in various hydrodynamic situations has been analyzed in a number of papers, among which we will cite [1-6]. Flexible macromolecules are modeled by dumbbells with identical "spheres" and a nonlinear elastic link between them. If we neglect the inertial forces, then, as a consequence of the low macromolecular mass, it is possible to have

$$\overline{F}_1 + \overline{F}_f + \overline{F}_B + \overline{F}_{iv} = 0. \tag{1}$$

The elastic force $\overline{F}_1 = -3Nk\theta\,\mathcal{L}(r'/R)\overline{r}'/R^2$. For the nonlinear function $\mathcal{L}(r'/R)$ we take the Warner approximation $\mathcal{L}(r'/R) = [1 - (r'/R)^2]^{-1}$. With such an approximation the elastic force sharply increases in proportion to the straightening of the circuit and tends toward infinity as $r' \to R$, which is in accord with physical sense (for any conformation of the circuit, the length of the "head-to-tail" vector of the macromolecule cannot be greater than the length of the totally straightened circuit). The force of hydrodynamic friction which arises as a consequence of the relative motion of the solution and the spheres of the "dumbbell" is given by $\overline{F}_f = \xi(r'/R)(\overline{v} - \overline{r}')$. The parameter of external friction, a function of the conformation of the circuit, is taken [5, 6] to be equal to $\xi = \xi_0 Q(r'/R) = \xi_0\sqrt{Nr'/R}$;

A. V. Lykov Heat and Mass Transfer Institute, Academy of Sciences of the Belorussian SSR, Minsk.

Translated from Inzhenerno-Fizicheskii Zhurnal, Vol. 55, No. 5, pp. 743-750, November, 1988. Original article submitted June 2, 1987.

0022-0841/88/5505-1223$12.50

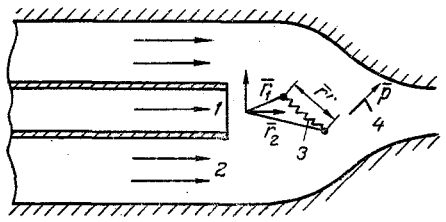

Fig. 1. Flow diagram: 1) flow of macromolecule solution; 2) flow of dispersion medium; 3) flexible macromolecule; 4) rigid macromolecule.

the velocity $v_i = G_{ij}x_j$. The statistical Brownian force exerted on the "spheres" of the dumbbell is given by $\bar{F}_B = -k\theta\nabla \ln \psi$. The force of internal friction F_{iv} in the macromolecule is proportional to the rate of deformation, i.e., $F_{iv} = -\varphi/N(\dot{\bar{r}}' - \bar{\Omega} \times \bar{r}')$. The quantity Ω can be determined from the fact that the resulting moment of the internal friction forces is equal to zero, i.e., $\sum_{i=1}^{2} \bar{R}_i \times \bar{F}_{iv} = 0$, which yields $\bar{F}_{iv} = -\varphi/N(\bar{r}'\bar{e}_r)\bar{e}_r$.

In deriving the equations for the moments $\langle x_i x_j \rangle$ we have to determine the form of the probability-density function $\psi(t, \bar{r}')$. The equation of conservation (the Liouville equation) for this is

$$\frac{\partial \psi}{\partial t} + \nabla(\dot{\bar{r}}'\psi) = 0. \tag{2}$$

With the chosen type of functional relationship for the forces included in Eq. (1), the sought quantity $\dot{\bar{r}}'$ is equal to

$$\begin{aligned} \dot{\bar{r}}' = &-\frac{k\theta}{\xi}\left[\nabla \ln \psi - \frac{\varphi/N}{\varphi/N + \xi}(\bar{e}_r \nabla \ln \psi)\bar{e}_r\right] - \\ &- \frac{3Nk\theta\bar{e}_r}{(\xi + \varphi/N)[1 - (r'/R)^2]}\frac{r'}{R} + \bar{G}\bar{r}' - \frac{\varphi/N}{\varphi/N + \xi}(\bar{e}_r \bar{G}\bar{r}')\bar{e}_r. \end{aligned} \tag{3}$$

Let us derive the equation for the second-order moments $\langle x_i x_j \rangle$. The averaging is accomplished with utilization of the distribution function. Utilization of (2) and (3) after algebraic transformations leads to the following equations for the moments:

$$\begin{aligned} \frac{d}{dt}\langle x_i x_j \rangle = 2k\theta &\left[\left\langle \frac{\delta_{ij}}{\xi} \right\rangle - \left\langle \left\{ \frac{1}{\xi^2 r}\frac{d\xi}{dr} + \frac{1}{r^4}\frac{d}{dr}\left[\frac{1}{\xi} \times \right.\right.\right.\right. \\ &\left.\left.\left.\left. \times \frac{\varphi/N}{\varphi/N + \xi}\right]\right\} x_i x_j \right\rangle\right] - \frac{6Nk\theta}{R^2}\left\langle \frac{x_i x_j}{(\xi + \varphi/N)[1 - (r'/R)^2]} \right\rangle - \\ &- 2\left\langle \frac{\varphi/N}{\varphi/N + \xi}\frac{x_\alpha x_\beta G_{\alpha\beta} x_i x_j}{\bar{r}'^2} \right\rangle + G_{\alpha n}(\langle x_j x_n \rangle \delta_{i\alpha} + \langle x_i x_n \rangle \delta_{j\alpha}), \end{aligned} \tag{4}$$

$$i, j = 1, 2, 3.$$

The resulting equation includes the function $\xi = \xi(r'/R)$, whose value is dependent on the conformation of the flow circuit. Two averaging methods are possible: substitute the explicit expressions for $\xi = \xi(r'/R)$ into Eq. (4) and then do the averaging, or assume that $\xi = \xi(\langle r' \rangle/R)$. For the numerical solution selected for this paper, we have chosen the second method, although we should point out that the first version presents no fundamental difficulties. For purposes of closing Eqs. (4), the fourth-order moments are expressed in terms of second-order moments. In addition, in analogy with the selected method of averaging for the terms containing $\xi(r'/R)$, for the Warner function we assume that $1 - (r'/R)^2 = 1 - \langle r'^2 \rangle/R^2$. The system of equations (4) is expanded to include the initial conditions at which $t = 0$;

$$\langle x^2 \rangle = \langle y^2 \rangle = \langle z^2 \rangle = R^2/[3(N+1)], \quad \langle xy \rangle = \langle xz \rangle = \langle yz \rangle = 0 \tag{5}$$

(in its original state the macromolecular solution was at rest). Analysis of problem (4)-(5) shows that under conditions of elongational flow, when only the nondiagonal components in the tensor G_{ij} are different from zero, with macromolecular deformation the diagonal components of the tensor $a_{ij} = \langle x_i x_j \rangle$ remain equal to zero.

Introduction of the dimensionless variables and parameters $\tilde{r} = r'/R$, $\tilde{\xi} = \xi/\xi_0$, $\tilde{\varphi} = \varphi/\xi_0$, $\alpha = \nu\tau$, $\tau = \xi_0 R^2/(6Nk\theta)$, $\tilde{z} = z'/a_0$, $V = u_z/v_{in}$, $\nu = v_{in}/a_0$ as well as the transition to the Euler coordinate system from the Lagrange system of coordinates connected to the macromolecule (the Euler system is the laboratory system) (the sign ~ is dropped) reduces problem (4)-(5) to

$$\frac{d\langle x_i^2\rangle}{dz} = \left\{\frac{1}{3NQ} - 2\langle x_i^2\rangle\left[\frac{1}{2Q}\,\frac{\varphi/N}{\varphi/N+Q}\,\frac{1}{\langle r'^2\rangle} + \right.\right.$$
$$\left.\left. + \frac{1}{2(\varphi/N+Q)}\,\frac{1}{1-\langle r'^2\rangle} + \frac{\varphi/N}{\varphi/N+Q}\,\alpha\,\frac{\langle x_j^2\rangle}{\langle r'^2\rangle}\,\Gamma_{jj}\right] + 2\alpha\langle x_i x_n\rangle\Gamma_{in}\right\}/V\alpha, \quad i = 1, 2, 3, \tag{6}$$

where

$$\Gamma_{ij} = \lambda\begin{pmatrix} -1/2 & 0 & 0 \\ 0 & -1/2 & 0 \\ 0 & 0 & 1 \end{pmatrix}$$

and

$$\langle x_i^2\rangle = 1/[3(N+1)] \text{ when } t = 0. \tag{7}$$

System (6), (7) was solved numerically.

The calculations were carried out for three types of convergent nozzles. The contour for the type a nozzle was formed from two circular sections which make a smooth transition into each other; for the type b nozzle the contour is described by a single curve; in the case of c the nozzle was formed as a straight line touched on a circular section. In each of these cases the dimensions were kept constant and equal to D = 1.5 mm, d_c = 0.15 mm, and L = 8 mm, which made it possible to carry out the comparative analysis.

The geometry of the convergent channels is given by

$$\text{a) } r = \begin{cases} \sqrt{3136 - z^2} - 55 & (0 \leqslant z \leqslant 9.733); \\ 5.7 - \sqrt{31.36 - (10.67 - z)^2} & (9.73 < z \leqslant 10.671); \end{cases}$$

$$\text{b) } r = 0.1 + 0.9\,(1 - z/10.67)^2;$$

$$\text{c) } r = \begin{cases} 1 - 0.0875z & (0 \leqslant z \leqslant 9.55); \\ 12.53 - \sqrt{12.43^2 - (10.67 - z)^2} & (9.55 < z \leqslant 10.67). \end{cases}$$

The calculations were performed both within the geometric cell where $\lambda \geq 0$, as well as within the escaping jet where there is no deformation ($\partial u/\partial z = 0$ and therefore $\lambda = 0$). The values of λ and V were determined from the solution of the hydrodynamic problem for a corresponding type of cell. Some of the results from these calculations are shown in Figs. 2-3. In these calculations, we varied the parameters of the macromolecules (N) and of the De Boer number (α).

At the inlet to the hydrodynamic cell the macromolecules are found in the form of a clump, where the square of the length of the "head-to-tail" vector of the macromolecule, according to (7), is equal to $(N + 1)^{-1}$, while the second-order moments $\langle x^2\rangle$, $\langle y^2\rangle$, $\langle z^2\rangle$ are equal. As the flexible macromolecule moves along the axis of the cell, it begins to unwind and simultaneously orient itself (the distribution of the second-order moments loses its equiprobable distribution). However, the rates of these conversions vary at different sections of the hydrodynamic cell. At the initial section of the cell the macromolecule is virtually free of any deformation as long as the quantity λ does not exceed its threshold value (Fig. 2). This is then followed by swift stretching out of the macromolecule. As the De Boer number increases (for example, as a result of an increase in ν, i.e., with a reduction in the characteristic time of the process as a consequence of an increase in the discharge rate), this stage of swift growth sets in all the more rapidly (Fig. 2a). Having attained the maximum level of elongation within the cell, the macromolecules virtually do not change in length all the way to the outlet from the cell. Beyond the limits of the cell begins the coagulation of the macromolecules, since the tensile stresses generated by the presence of a longitudinal velocity gradient are absent. In this case, the smaller the De Boer number, the more rapid the deflection of the macromolecules. This is brought about by the fact that with unchanging macromolecule properties (the value of the time τ is fixed),

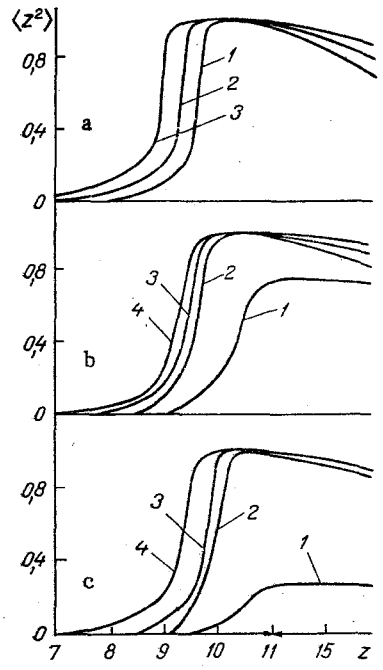

Fig. 2

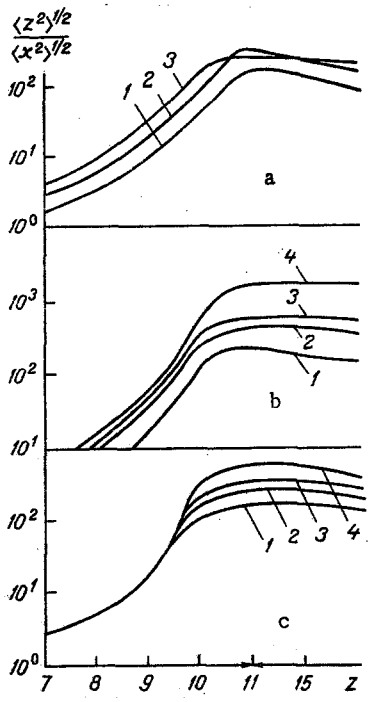

Fig. 3

Fig. 2. Second-order moment as a function of the longitudinal coordinate (for cell-type a) with a change in the De Boer number (a): 1) $\alpha = 0.3$; 2) 1; 3) 3; with a change in the macromolecule lengths for corresponding changes in α (b) as well as for const ($\alpha = 1$) (c): 1) N = 10,000; 2) 1,000; 3) 500; 4) 100.

Fig. 3. Macromolecule orientation as a function of the longitudinal coordinate with a change in the De Boer number (a): 1) $\alpha = 0.3$; 2) 1; 3) 3; macromolecule length with a corresonding change in α (b) and with $\alpha = 1$ (c): 1) N = 10,000; 2) 1,000; 3) 500; 4) 100.

the smaller α numbers correspond to the smaller flow velocities and, respectively, to greater lengths of stay within the flow.

If the macromolecule parameters change, for example, the length, i.e., the number N of circuit segments (with a fixed segment length a), then with a constant discharge this denotes the simultaneous variation of the α number as well. Here, both the coordinate origin of intensive deformation and the rate of reverse macromolecule coagulation are shifted (Fig. 2b). In the case of very long macromolecules, they do not have enough time to develop completely, but beyond the cell over a distance of ten calibers they exhibit virtually no deflection.

With a simultaneous change in both the macromolecule parameters (the number n) and in the discharge in such a way that the De Boer number remains constant (Fig. 2c), these trends become even more pronounced. The fact of the matter is that the discharge must diminish in proportion to the increase in N, which leads to a reduction in the stresses acting from the fluid on the macromolecule.

Pronounced orientation of the macromolecule also occurs within the flow, i.e., asymmetry of the second moments appears (at the inlet to the cell $\langle z^2\rangle^{1/2}/\langle x^2\rangle^{1/2} = 1$) (Fig. 3). In this case, unlike the function $\langle z^2\rangle$ no plateau of the function $\langle z^2\rangle^{1/2}/\langle x^2\rangle^{1/2}$ is observed. This indicates that the macromolecule which is already virtually completely straightened will only orient itself in the future. Let us note that the maximum degree of orientation is not achieved at the outlet from the convergent channel, but somewhat closer to it. This comes about because the velocity gradient also attains its extreme value within the convergent channel. As a rule, with an increase in the De Boer number, the

degree of asymmetry for the distribution of second moments increases (Fig. 3a). However, it is also possible for the curves to intersect at sufficiently large De Boer numbers (the calculations have been carried out for cells of the a type). This is explained by the fact that the absolute values of the longitudinal velocity gradients increase with an increase in the discharge rate, and consequently, in the stresses acting on the macromolecule. But with this there is a reduction in the time of this effect. The competition between these given factors leads to a situation in which, sometimes, the reduction in the stay time exerts a decisive effect, and then the degree of macromolecule orientation begins to fall with an increase in the De Boer number.

The degree of macromolecule orientation depends strongly on the lengths of the macromolecules. Figure 3b shows this relationship for a fixed discharge flow rate, so that the De Boer number changes in proportion to N (a cell of the a type). Let us note that large macromolecules even in the free streams at the outlet from the nozzle remain markedly oriented.

If with an increase in the number of links (i.e., the relaxation time τ) there is a proportional increase in the stay time within the convergent channel (as a result of a reduction in the discharge flow rate) such that α = const, this will compensate the strengthening of the degree of orientation as a consequence of the increase in N for virtually the entire convergent nozzle. However, in the region of greatest flow compression there will, nevertheless, appear the factor of circuit length (Fig. 3c) (the curves are shown for a type c cell).

Rigid Macromolecules. We examine the dilution of a suspension of rigid axisymmetric particles free from external mass forces or couples, and of sufficiently small size to permit us, in analyzing the microdynamics, to neglect inertia. An isolated particle is connected to the unit vector $\bar{p}(t)$ directed along the axis of particle symmetry. If we place this particle into a time-dependent uniform linear flow

$$\bar{u}(\bar{r}, t) = \tilde{G}(t)\,\bar{r},$$

where $\tilde{G} = \tilde{E} + \tilde{\Omega}$, $\tilde{E}^T = \tilde{E}$, $\tilde{\Omega}^T = -\tilde{\Omega}$, the particle will rotate in the absence of Brownian couples in accordance with the following equation [7]:

$$\frac{d\bar{p}}{dt} = \tilde{\Omega}\bar{p} + \lambda_1 [\tilde{E}\bar{p} - \bar{p}(\bar{p}\tilde{E}\bar{p})]. \tag{8}$$

When there are Brownian couples present, the orientation of a single particle is defined by the statistical probability-density function $N(\bar{p}, t)$ which satisfies the Fokker–Planck equation in space $\bar{p}$:

$$\frac{\partial N}{\partial t} + \nabla\left[N\frac{d\bar{p}}{dt} - D\nabla N\right] = 0. \tag{9}$$

Equations (8) and (9) describe the evolution of the microstructure; in particular, from these we obtain the relationships for the second-order moments [7]:

$$\frac{d\langle p_i p_j\rangle}{dt} = \Omega_{ik}\langle p_k p_j\rangle - \langle p_i p_k\rangle\Omega_{jk} + \lambda_1[E_{ik}\langle p_k p_j\rangle + \langle p_i p_k\rangle E_{jk} - 2\langle p_i p_j p_\alpha p_k\rangle E_{\alpha k}] - 6D[\langle p_i p_j\rangle - \delta_{ij}/3]. \tag{10}$$

Equations (10), defining the dynamics of the quantity $\langle\overline{pp}\rangle$, contain the unknown higher moment $\langle\overline{pppp}\rangle$. In analogous fashion we can derive the equation which defines the change in time for any finite moment $\bar{p}$ relative to the vector, but in each such equation we must include a higher moment $\bar{p}$.

In principle, we can solve Eq. (9) for the distribution function $N(\bar{p}, t)$ of a given type of flow and with its aid to determine the second-order moments. However, as indicated in [7], only the limit cases of very weak or very strong flows, corresponding to almost nearly equilibrium or, conversely, strongly nonequilibrium microstructures, lend themselves to rigorous asymptotic solution. In the case of a flow of arbitrary intensity, we must proceed in a different way, i.e., one in which an infinite chain of moment equations such as (10) is broken at the quadratic level by means of a simple interpolation procedure for the expression $\langle\overline{pppp}\rangle$ in terms of $\langle\overline{pp}\rangle$. Following [7], we select the form of the link between the fourth-order and second-order moments to be as follows:

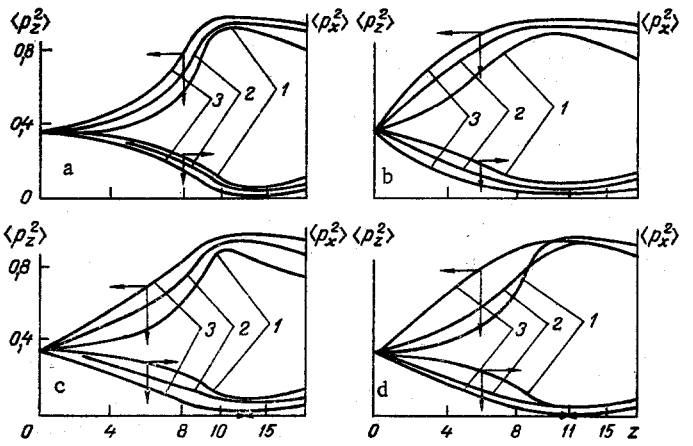

Fig. 4. Second-order moments of the orientation vector as a function of the longitudinal coordinate with a change in the De Boer number: 1) $\alpha = 0.3$; 2) 1; 3) 3 (*a* is a cell of the a type, b is a cell of the b type, c is a cell of the c type) and with variation of the cell type ($\alpha = 1$): 1) cell type a; 2) cell type c; 3) cell type b.

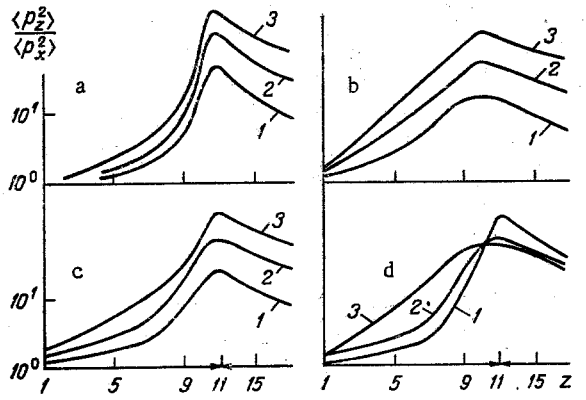

Fig. 5. Degree of orientation as a function of the longitudinal coordinate with a change in the De Boer number: 1) $\alpha = 0.3$; 2) 1; 3) 3 (*a* is the a-type cell; b is the b-type cell; c is the c-type cell) and with variation of cell type ($\alpha = 1$): 1) a-type cell; 2) c-type cell; 3) b-type cell.

$$\langle p_i p_j p_\alpha p_k \rangle E_{\alpha k} = \frac{1}{5} [6 \langle p_i p_\alpha \rangle E_{\alpha k} \langle p_k p_j \rangle - \langle p_i p_j \rangle \langle p_\alpha p_k \rangle E_{\alpha k} - 2\delta_{ij} \langle p_\alpha p_k \rangle^2 E_{\alpha k} + 2\delta_{ij} \langle p_\alpha p_k \rangle E_{\alpha k}]. \quad (11)$$

Presenting the fourth-order moments in this way makes it possible, first of all, to accomplish the transition to the limit cases of both weak and strong flows, and secondly, to satisfy the condition $\mathrm{tr}\langle p_i p_j \rangle = 1$. In the light of the fact that in elongational flows $\Omega_{ik} = 0$, with the following initial conditions

$$\langle p_i^2 \rangle = 1/3, \quad i = 1, 2, 3; \quad \langle p_i p_j \rangle = 0, \quad i \neq j, \quad (12)$$

all second-order moments $\langle p_i p_j \rangle$ with $i \neq j$ retain zero values throughout the entire deformation period. The displacement velocity tensor

$$E_{ih} = \nu\lambda \begin{pmatrix} -1/2 & 0 & 0 \\ 0 & -1/2 & 0 \\ 0 & 0 & 1 \end{pmatrix},$$

since there is symmetry with respect to the components x, y.

Transition to dimensionless variables in the laboratory coordinate system leads us to the following system of equations:

$$\frac{d\langle p_x^2\rangle}{dz} = \left[\lambda_1\lambda\alpha\left\{-\langle p_x^2\rangle + \frac{2}{5}\left[2(\langle p_z^2\rangle^2 - \langle p_z^2\rangle + \langle p_x^2\rangle) + \right.\right.\right.$$
$$\left.\left.\left. + \langle p_x^2\rangle\langle p_z^2\rangle\right\} - \langle p_x^2\rangle + \frac{1}{3}\right]/(V\alpha);$$
$$\frac{d\langle p_z^2\rangle}{dz} = \left[\lambda_1\lambda\alpha\left\{2\langle p_z^2\rangle - \frac{2}{5}\left[3\langle p_z^2\rangle^2 + \langle p_z^2\rangle\langle p_x^2\rangle + 2\langle p_j^{ii}\rangle^2 + \right.\right.\right.$$
$$\left.\left.\left. + 2(\langle p_z^2\rangle - \langle p_x^2\rangle)\right]\right\} - \langle p_z^2\rangle - 1/3\right]/(V\alpha). \qquad (13)$$

Some of the results from the numerical solution of problems (12) and (13) are shown in Figs. 4 and 5. The calculations were conducted for an extended ellipsoid exhibiting an axis ratio of $a/b = 7$. Here we have a coefficient of the form $\lambda_1 = 0.96$ (an increase in the degree of anisodiametricity of the particles has virtually no effect on the results of the numerical solution). As before, the De Boer number has a decisive effect on the dynamics of deformation. Rigid macromolecules manage to "accumulate" beneath the external flow, so that the large orientation (Fig. 4) corresponds to the large De Boer numbers. The flexible macromolecules must not only be oriented, but they change their characteristic dimensions, which results in their visual persistence. The rate of growth in the macromolecule "orientability" is strongly dependent on the geometry of the convergent nozzle. At the inlet section we find the maximum orientation corresponding to a cell of the b type; however, the most pronounced orientation effects are noted at the outlet from the convergent channel in the case of flow in cell a. As we penetrate deeper into the convergent channel, we note an increase in the degree of asymmetry for the distribution of the second moments. As a consequence of the fact that the rigid macromolecules, unlike the flexible macromolecules, do not change their length as a result of deformation, their degree of orientation is substantially less than in the case of flexible macromolecules. This is confirmed by comparison of the results shown in Figs. 3 and 5. At the outlet from the convergent channel (flow in a free jet) the rigid macromolecules are more markedly disoriented, which is also explained by their relatively small length (in comparison to the flexible macromolecules).

In Fig. 5d we find a comparison of the orientations for the macromolecules in flows through various types of convergent channels. Since the rates of flow compression in a type b nozzle are maximum at the inlet segment, there is a corresponding maximum macromolecule orientation, but as has already been mentioned earlier, in conclusion, a nozzle of the a type is much to be preferred.

NOTATION

N is the number of statistical segments in the macromolecule; a, segment length; k, Boltzmann constant; θ, temperature; $R = Na$, length of the macromolecule in the completely straightened state; $\bar{r}'$, head-to-tail vector of the macromolecule; $\bar{v}$, velocity of the dispersion medium; Ω, angular speed of macromolecule rotation; x_i, projection of the $\bar{r}'$ vector onto the i axis; ξ_0, normed parameter of external friction; φ, internal friction parameter; a_0, initial diameter of the convergent channel; v_{in}, velocity of the dispersion medium at the inlet to the convergent channel; $\tilde{G}$, velocity-gradient tensor; $\tilde{E}$, strain-rate tensor; $\tilde{\Omega}$, vortex tensor; λ_1, shape factor (for an ellipsoidal particle $\lambda_1 = (a^2 - b^2)/(a^2 + b^2)$, where a and b are the major and minor semiaxes. The superscript T denotes the transposed tensor.

LITERATURE CITED

1. Yu. Ya. Gotlib, A. A. Darinskii, and Yu. É. Svetlov, Physical Kinetics of Macromolecules [in Russian], Leningrad (1986).
2. R. I. Tanner and W. Stehrenberger, J. Chem. Phys., 55, No. 4, 1958-1964 (1971).
3. R. I. Tanner, Trans. Soc. Rheol., 19, No. 1, 37-65 (1975).
4. R. I. Tanner, Trans. Soc. Rheol., 19, No. 4, 557-582 (1975).
5. N. Phan-Thien and R. Tanner, Rheol. Acta, 17, No. 6, 568-577 (1978).
6. G. G. Fulleer and L. G. Leal, Rheol. Acta, 19, No. 5, 580-600 (1980).
7. F. J. Hinch and L. G. Leal, J. Fluid Mech., 76, No. 3, 187-206 (1976).

ACOUSTIC FLOWS AND ACOUSTOOPTIC INTERACTION IN A GASEOUS MEDIUM

V. I. Zagorel'skii, D. O. Lapotko, O. G. Martynenko, and G. M. Pukhlov

UDC 534.286:535.421

The formation of secondary flows generated when intensive ultrasonic waves are propagated and absorbed in a gaseous medium is investigated experimentally. The effect of acoustic flows and sound absorption on acoutooptic interaction for diffraction of light on acoustic waves in a gas is investigated.

The propagation with absorption of large-amplitude acoustic waves results in the formation of intensive secondary flows (acoustic wind) in the region of the acoustic beam [1]. The investigation of such flows in a gas is of independent interest and is also of interest in connection with the need to study the effect of the acoustic wind on different processes coinciding with it in space and time. Thus, in realizing diffraction of light on ultrasonic waves in a gaseous medium for the purpose of active influence on the light radiation one needs high-frequency, high-intensity acoustic fields [2]. In this case the frequency and intensity of the sound are large enough to result in its absorption and the development of secondary acoustic flows in the medium. The existing theories of diffraction of light on acoustic waves [3, 4] do not allow one to take account of the acoustic wind, because they are oriented toward condensed acoustooptic media in which such flows are either negligibly small or do not arise at all.

In the present work the development of the acoustic wind arising when ultrasonic waves with frequency equal to 1 MHz are absorbed and the effect of secondary flows on acoustooptic interaction in the Bragg regime are investigated experimentally. Air and xenon at atmospheric pressure are used as a working medium. The sound was radiated into the gas by pulses of duration up to 1 sec and intensity up to 140 dB. Dissipative phenomena that arise in the propagation of acoustic waves were investigated by shadow methods on the IAB-451 apparatus. Since a variation in the velocity of the medium in the propagation of sound is spatially related to a variation in its temperature, the intensity of the flows was estimated from the angle of deflection of light in a shadow device ε measured directly in the experiment.

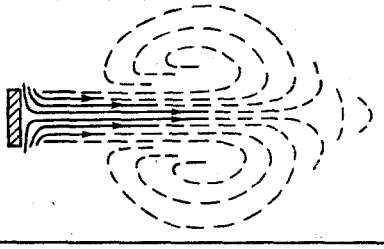

Fig. 1. Secondary acoustic flows near the acoustic radiator.

A. V. Lykov Institute of Heat and Mass Exchange, Academy of Sciences of the Belorussian SSR, Minsk. Translated from Inzhenerno-Fizicheskii Zhurnal, Vol. 55, No. 5, pp. 751-754, November, 1988. Original article submitted November 4, 1987.

 0022-0841/88/5505-1230$12.50